Energy partitioning in atom–radical reactions: The reaction of F atoms with NH2

D. J. Donaldson, J. J. Sloan, and J. D. Goddard

Citation: The Journal of Chemical Physics **82**, 4524 (1985); doi: 10.1063/1.448707
View online: http://dx.doi.org/10.1063/1.448707
View Table of Contents: http://scitation.aip.org/content/aip/journal/jcp/82/10?ver=pdfcov
Published by the AIP Publishing

Energy partitioning in atom–radical reactions: The reaction of F atoms with NH_2

D. J. Donaldson[a] and J. J. Sloan[b]
Division of Chemistry, National Research Council of Canada, Ottawa, Ontario, Canada K1A 0R6
J. D. Goddard
Guelph–Waterloo Centre for Graduate Work in Chemistry, Department of Chemistry and Biochemistry, University of Guelph, Guelph, Ontario, Canada N1G 2W1

(Received 13 December 1984; accepted 29 January 1985)

An extension of the low-pressure infrared chemiluminescence technique has allowed the measurement of energy partitioning in the atom/radical reactions: $F + NH_2 \rightarrow HF + NH$, $F + ND_2 \rightarrow DF + ND$. A complete numerical model of the experiment is described in detail including its parametrization. This model allows the unambiguous determination of the primary energy distribution of the above reactions. These reactions give inverted product energy distributions, in contrast to the isoelectronic $F + OH \rightarrow HF + O$ reaction. The inverted primary energy distribution for $F + NH_2/ND_2$ indicates a direct abstraction mechanism. *Ab initio* quantum chemical computations on some features of the relevant potential energy surfaces support this direct abstraction route. An energetically accessible transition state, having approximately zero barrier, is found on the triplet surface which directly correlates reagents and products. The geometry of this triplet transition state is also suggestive of strong HF vibrational excitation. Abstraction on the triplet surface provides an alternative pathway to reaction on the lowest singlet surface, which contains a deep potential energy well corresponding to NH_2F.

I. INTRODUCTION

We have recently developed an apparatus for the measurement of energy partitioning in atom/radical reactions, based on an extension of the low-pressure infrared chemiluminescence technique. In this experiment, substantial concentrations of radicals are generated at submillitorr pressure in the gas phase by the abstraction of a hydrogen atom from a suitable molecular precursor, in the reaction of the latter with an F atom. These hydrogen abstraction reactions are very fast; most have rate constants greater than 10^{-11} cm^3 $molecule^{-1}$ s^{-1}. As a result, a substantial fraction of the precursor molecules can be converted to radicals in a properly designed apparatus, even at total pressures as low as $1–5 \times 10^{-3}$ Torr. The reactions of the radicals so generated are studied using standard low-pressure infrared chemiluminescence techniques.

In the present case, the precursor molecule is NH_3, and the reaction which generates the radicals is

$$F + NH_3 \rightarrow HF(v' \leqslant 2) + NH_2, \quad \Delta H_0^0 = -30 \text{ kcal mol}^{-1}. \tag{1}$$

This reaction is followed by:

$$F + NH_2 \rightarrow HF(v' \leqslant 4) + NH, \quad \Delta H_0^0 = -43 \text{ kcal mol}^{-1}. \tag{2}$$

The analogous isotopically substituted reactions:

$$F + ND_3 \rightarrow DF(v' \leqslant 3) + ND_2 \tag{3}$$

and

$$F + ND_2 \rightarrow DF(v' \leqslant 5) + ND \tag{4}$$

were also examined.

The energy distributions from the precursor reactions (1) and (3) have been reported in previous publications.[1–3] Since the secondary atom/radical reactions [(2) and (4)] are extremely fast, it is difficult to eliminate them by conventional experimental techniques. This interference presents serious difficulties, because reactions (2) and (4) populate nearly the same product vibrational levels as reactions (1) and (3), respectively, yet—as will be shown in later sections of this paper—give substantially different product vibrational excitation. As a result, extreme variations in the observed product vibrational distributions have been reported, and widely differing primary energy distributions for the atom/molecule reactions have been suggested.[2–4]

We have recently completed a reinvestigation of the primary reactions,[5] in which we have identified the primary energy distributions in reactions (1) and (3). In the course of that study, it became necessary to separate the primary and secondary energy distributions unambiguously, and to measure both. By carrying out a large number of experiments under conditions (to be described later) where the secondary reaction could be induced, we were able to identify qualitative changes in the energy distribution which could be associated with its occurrence. These observations permitted us to identify those experiments in which the secondary reactions did not contribute to the observed HF chemiluminescence, and hence to obtain correct primary energy distributions for reactions (1) and (3).

For the purposes of this work, it was necessary to write a complete numerical model of the experiments, including descriptions of the gas dynamics and of all reactive and energy transfer processes involving the observed product (HF). After calibration, this model predicted changes in the ob-

---

[a] Department of Chemistry, University of Colorado, Boulder, Colorado 80309.

[b] Author for correspondence. Issued as NRCC No. 23771.

0021-9606/85/104524-13$02.10

served energy distributions resulting from variations in reagent flow and apparatus configuration to well within the error of the measurment. This model was used to extract the energy distributions for the secondary reactions from those measured results which contained contributions from both the primary and secondary processes. The numerical simulation, and the (calculated) primary energy distribution for the secondary reactions are reported below.

It became clear early in the course of the work reported in Ref. 5, that both secondary reactions [(2) and (4)] give strongly inverted product vibrational distributions. In the context of energy distribution measurements on similar reactions, this result is unusual. It has been found that similar atom/radical reactions (e.g., $F + HO \rightarrow HF + O$) occurring on potential energy surfaces containing a deep potential well corresponding to a strongly bound, stable molecule, frequently yield "cold" (noninverted) product vibrational distributions.[6–8] In such cases, the formation of a long-lived intermediate corresponding to the (highly energized) molecule, permits the randomization of the reaction exoergicity among all available product degrees of freedom. Under these circumstances it can be shown that an inverted product vibrational distribution is impossible.[9]

The inverted product energy distribution observed for the $F + NH_2 \rightarrow HF + NH$ reaction differs from that obtained for its isoelectronic analog: $F + OH \rightarrow HF + O$. *Ab initio* calculations for the latter[6] showed that the barrier on the lowest triplet surface (which correlates directly with the products) is not energetically accessible to the reagents. Consequently, the HF observed from the F + OH reaction must be the product of a nonadiabatic process in which the reagents enter on the bound singlet surface (leading to the FOH molecule) then, in the exit channel, cross to the triplet surface which correlates with the observed products. In this process, they sample that part of the surface corresponding to the strongly bound FOH intermediate. The lifetime of the latter is long enough to permit the randomization of the reaction exoergicity among the available product channels, leading to the observed (cold) product vibrational distribution.

The strongly inverted primary energy distributions measured for the $F/NH_2(ND_2)$ systems thus differed qualitatively from those found in other atom/radical reactions measured in this laboratory.[6–8] We therefore undertook *ab initio* calculations of relevant portions of the F/NH_2 potential energy surfaces to determine whether some energetically accessible reaction path exists which does not pass through a bound FNH_2 intermediate. A suitable transition structure was found; the results of these *ab initio* computations are also reported in this paper.

In the following sections of this paper, the experimental measurements and numerical simulations relevant to reactions (2) and (4) will be reported. The vibrational distribution for reaction (2) will be obtained from this information. Finally, the details of the *ab initio* calculations will be given. The quantum chemical computations show that strongly inverted vibrational energy distributions are expected for reactions (2) and (4), due to the existence of an energetically accessible transition state on a triplet surface which directly correlates the reagents and products without the necessity of forming any bound intermediate.

II. EXPERIMENT

The apparatus has been extensively described in Ref. 5. A block diagram of the reagent inlet and the main vacuum chamber is shown in Fig. 1. The reagent inlet is designed to accomplish the most efficient mixing of the atomic and molecular reagents. It consists of three concentric Teflon-coated quartz tubes located in the center of the top of the (cylindrical) reaction chamber lid. The atomic reagents, labeled A_1 and A_2 in Fig. 1, flow down the two outer tubes. In the following, the tubes containing A_1 and A_2 will be called tubes 1 and 2, respectively. For the present experiments, both A_1 and A_2 are F atoms formed from microwave discharges in SF_6 or CF_4. Either, or both discharges may be used for specific experiments.

In order to obtain efficient mixing of the atomic and molecular reagents, the latter, labeled M in Fig. 1, is injected laterally outward from a cylindrical opening in the wall of the central tube (the injector) at its lower end. This injection point can be moved vertically over a distance of about 4 cm from about 1 cm inside to about 3 cm below the end of tube 2.

The reaction chamber is evacuated by a 15 in. diffusion pump through a high-throughput cyrobaffle which was especially designed to permit the retention of about 6000 l/s. of the diffusion pump's speed at the bottom of the reaction chamber. For reagent flows in the range of 0.5–50 μmol/s, as used in this experiment, the resulting (average) pressure at the center of the reaction chamber is in the 10^{-3} to 10^{-5} Torr range. Since the reagents enter at the top of the reaction vessel, the large pumping speed creates a very strong pressure gradient between this point and the entrance to the cryobaffle, where the gases are removed. In addition, of course, a rapid drop in the partial pressure of the atomic reagent occurs as it leaves the quartz tube which delivers it to the reaction zone (the region surrounding the injector tip

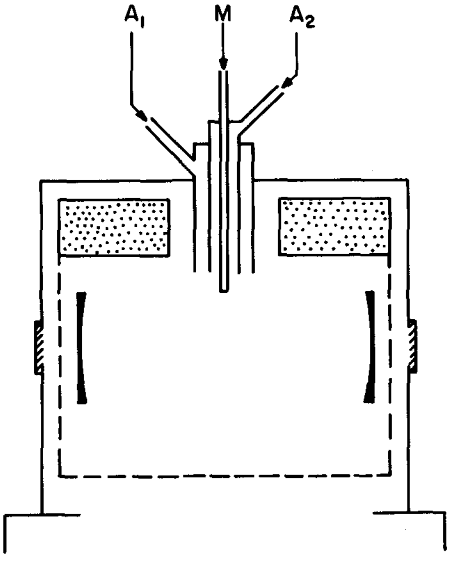

FIG. 1. Cross sectional sketch of reaction chamber showing three concentric reagent inlet tubes at top. The movable injector is the central tube. Dotted area is liquid nitrogen reservoir, dashed line shows volume enclosed by cold radial chevron cryobaffle. Curved surfaces show optical cell mirrors.

where the reagents mix). As a result, the apparatus can sample a very large range of reagent densities when the injector tip is moved over its vertical range.

The simulation calculations to be reported later indicate that the pressure range which can be sampled in this way covers nearly two orders of magnitude, as demonstrated by the variation of the total observed emission intensity and of the energy distribution of the "calibration" reaction: $F + H_2 \rightarrow HF + H$ with changes in the injector location. (The $F + H_2$ reaction was used to determine the parameters in the numerical model.) When the injection point is moved closer to or inside tube 2, it is observed that the emission intensity increases (by as much as two orders of magnitude, depending upon the flows) and the HF vibrational distribution becomes less inverted, due to relaxation in collisions with the walls of tube 2 and with the (higher pressure) reagent atoms inside the tube. These effects, which are quantitatively reproduced by the numerical model, will be discussed in detail in a later section.

If the reaction being studied has the possibility of a second step, then the extent of the latter is strongly enhanced when the injection point is withdrawn.[7] For the F/NH_3 and F/ND_3 systems, it is observed that when the injector is withdrawn, the HF vibrational distribution becomes sharply *more* inverted. This is opposite to the behavior observed for the F/H_2 reaction. However, in later sections, we show that this difference is due to the secondary reactions (2) and (4), which produce strongly inverted HF vibrational distributions. Hence their contribution makes the observed vibrational distribution more inverted.

The reagents used for this work are: CF_4 (Matheson, 97.5% purity), SF_6 (Air Products, 99.9% purity), H_2 and D_2 (Matheson, 99.95% purity), NH_3 (Matheson, 99.99% purity), and ND_3 (Merck Sharpe and Dohme, 99 atm % purity). All purities are as specified by the supplier. All results obtained on the systems reported here have been replicated using different reagent samples. No evidence of variation in the results due to impurities was found.

III. NUMERICAL MODEL

A. Description

A numerical model of the chemical processes and gas dynamics occurring in the reagent inlet and the reaction vessel has been written. This model uses the equations of intermediate or molecular flow (depending upon the local value of the Knudsen number) to calculate the flow of the gases inside tube 2, while numerically integrating the rate equations for the various contributions to the populations of the vibrational levels of the HF product. In the construction of the model, parameters are used to define processes which cannot be directly measured. The values of these parameters are determined by means of a multidimensional iterative procedure which minimizes the rms deviation between the calculated and measured values of a set of vibrational level populations and total emission intensities for the calibration reaction: $F + H_2 \rightarrow HF(v') \rightarrow H$.

The data set to which the calculation is compared in the iteration is obtained from 10–12 experiments, in each of which a distribution for this reaction is measured. Each of the experiments differs in the value of some variable—either a reagent flow, or the injector location. Variation of the reagent flows gives information on the various gas phase processes involving the reagents, while moving the injection point (hence the reaction zone) explores both the effect of changing reagent density and those effects which occur on the walls of the reagent inlet device. The experiments were therefore designed to test the ability of the numerical model to describe both gas phase and wall processes. It will be shown in the next section that all the measured data were accurately reproduced by the numerical model, suggesting that it contains correct descriptions of the important aspects of the experiment.

The purpose of this calculation is twofold. First, it is designed to provide a complete description of the low pressure experiment, based on simple chemical and physical laws. Therefore, it permits the detailed examination of any unusual results, such as those described in the Introduction for the F/NH_3 system, so that the origin of these may be determined. The second (and related) purpose is the estimation of the energy distributions for reactions which cannot be measured in isolation, such as reactions (2) and (4).

The energy distributions are calculated by numerical integration of the rate equations for all processes contributing to the population of each product vibrational state. The processes included in the calculation are: chemical reaction, gas phase vibrational deactivation by all species present (including the possibility of up-pumping an self-deactivation in collisions of two vibrationally excited products), infrared emission, and deactivation on the walls of tube 2. Five parameters are required to define those aspects of the model which cannot be directly measured. In the following, the mechanics of the calculation will be outlined, and these parameters will be identified.

The flow of F atoms is obtained from the total flow of F-atom precursor (measured during the experiment) by the use of a parameter N_d, which is the number of F atoms generated per precursor molecule in the microwave discharge. Following this step, the initial partial pressures of F atoms, undissociated precursor molecules, and radicals are calculated. In this, and all subsequent conversions from flow rate into instantaneous partial pressure, conservation of mass flow is used with the appropriate equations for the conductance of tube 2.[10] This calculation also yields the average bulk flow velocity.

In view of the construction of the injector tip (see Sec. II), it is assumed that the horizontal flux distribution of the injected molecular reagent is cylindrically symmetrical having, in the vertical dimension, a cosine distribution with its maximum at the injector tip. This assumes effusive flow from the injector, a condition met by the existing slot size and (measured) reagent pressure inside the injector tube. This assumption of effusive flow provides a convenient analytic starting point for the calculation of the reagent flux at any point surrounding the injector. The final computation of the vertical profile of the molecular reagent density uses different algorithms for the various regions inside and outside tube 2.

To obtain the partial pressure of the molecular reagent inside tube 2 at locations above the injection point, a conservation of mass flow condition is applied at each point above the injector tip. At each step of the calculation, the upward flow of molecular reagent through a cross section of the tube located at a given distance from the injection point is computed as described previously. This upward flux is then multiplied by the function $\exp(-1/1_m)$ where 1 is the distance from the injection point, and 1_m is the average local mean free path, to account for collisional attenuation by the downward-flowing gases. The resulting (upward) flow is equated to the downward flow of the same gas at the same point, since no gas escapes from the top of the tube, and the result is used to compute an instantaneous partial pressure, using the appropriate conductance equations. This procedure yields a numerical function of molecular reagent density vs distance inside tube 2. The density at locations below the injector is obtained simply by adding the reagent flowing downward from higher levels to that obtained by direct injection.

At one mean free path from the end of the tube, a transition region is entered. In this region, the conductance equations are switched to those for intermediate flow in a short tube (including the end effects),[10] and a function is switched on to describe the expansion (pressure decrease) as the gas emerges from the end of the tube.

This expansion is modeled assuming that the pressure decreases according to a Gaussian function having the form: $\exp[(-1/P_p)^2]$, where 1 is the distance, and P_p is a parameter giving the distance at which the pressure has fallen to $1/e$ of its value. This assumption is a great simplification of the actual expansion, which is influenced by such factors as the focusing effect due to flow from a long tube at low pressure,[11] and the lateral injection of the molecular reagent in the vicinity of the bottom of tube 2. However, these factors have opposite effects and the approximation introduced by the use of this Gaussian description seems acceptable, as will be seen.

The value of the parameter P_p is determined by the requirement that the calculated pressure, at a given distance from the injector, must coincide with the pressure measured at the same distance during the experiment. The pressure is measured with a calibrated ionization gauge mounted on the vacuum chamber wall at a measured distance from the injector. Conductance calculations indicate that these pressure measurements should be accurate to within a factor of 5, since the radial Chevron configuration of the baffles between the observation zone and the pressure gauge is relatively open. Although a factor of 5 in pressure would appear to be poor accuracy, it nevertheless serves to determine P_p quite well, because a factor of 5 change in the calculated final pressure results from a variation of only ± 5 mm. in the value of P_p. Hence, the experimental pressure measurements were quite valuable in determining the value of P_p.

The wall deactivation of the vibrationally excited HF product is parametrized, since the accomodation of vibrational energy at a surface is a complicated function of the state of the surface and the nature of the molecule–surface interactions. For the present purpose, the complete vibrational deactivation process is treated as a sum of two contributions—one in which the HF loses a single quantum of vibrational energy, and another in which it is completely deactivated to the ground ($v = 0$) state. Any arbitrary deactivation pattern can thus be represented by a mixture of these two processes. The rate for each is assigned a parameter. For the ($v \rightarrow v-1$) process, the parameter is K_w^{-1}. For the ($v \rightarrow v = 0$) process, the rate is given by the parameter K_w^0.

Under "normal" conditions (clean walls) the calculation shows that the ($v \rightarrow v = 0$) events do not occur for the $F + H_2$ reaction (i.e., $K_w^0 = 0$ for the best fit between measured and calculated distributions). However, for other experiments on $F + H_2$ in which the walls of the reagent inlet glassware had been previously coated with an efficient deactivator (NH_4F—*vide infra*), K_w^0 is found to be quite large. In both cases, excellent agreement with measured distributions was obtained using the assumption that K_w^0 is independent of vibrational level.

The ($v \rightarrow v-1$) rates, on the other hand, must depend on the vibrational level of the HF, since no acceptable fit could be obtained with the data if this dependence was neglected. This dependence was described using a scaling law based on measurements of HF(v) deactivation probabilities in collisions with large molecules.[12] It is found[12,13] that the vibrational deactivation rates for a large number of such molecules scale as a small power of the vibrational level. This power was treated as a parameter α_ω. In the calculations, the best fits were obtained when this parameter was between 2 and 3.

A total of five parameters are thus used in the model: $N_d, P_p, K_w^0, K_w^{-1}$, and α_w. As indicated previously, the reaction $F + H_2 \rightarrow HF + H$ was used in the initial optimization procedure which determined the parametrization of the model. In this procedure, three vibrational populations and one total emission intensity were measured for each of 11 experiments, giving a total of 44 data to be reproduced by the five parameters. In addition, total pressure measurements were made during all experiments, and the computed total pressures were required to match these. This requirement placed a strong constraint on the possible values of P_p, the parameter describing the pressure drop following reagent injection.

All gas phase energy transfer rate constants were taken from existing literature values.[13] Detailed rate constants for the primary reactions (1) and (3) were taken from product vibrational population measurements made using the lowest possible reagent partial pressures and furthest possible injector extension consistent with observation of a measurable signal.[5] Under these conditions, both gas phase deactivation and secondary reaction (between reagent atoms and radicals remaining from the primary reaction) are reduced to a minimum. The total rate constants used for the $F + H_2$ and $F + D_2$ reactions were 2.3×10^{-11} and 1.4×10^{-11} $cm^3/$molecule s, respectively.[14]

The steps in each calculation are as follows: Beginning at the top of tube 2, where the concentration of the molecular reagent is negligible, a sample of the gas is followed downward while the various contributions to the product vibrational populations are integrated. At the point where the sample reaches the light-collection optics (see Fig. 1), summation of the infrared emission (weighted by the efficiency function of the optical cell[16] is begun. This is continued until

TABLE I. Conditions for $F + H_2$ experiments used in calibration of numerical model.

Run	SF_6 flow[a]	H_2 flow[a]	Injector position[b]
11	1.03	1.24	− 1.75
12	1.41	1.41	0.0
13	1.41	1.56	0.65
14	1.58	4.76	0.65
15	1.66	4.91	0.0
16	1.55	5.06	− 1.75
17	1.63	1.36	− 1.75
18	4.30	1.44	− 1.75
19	4.38	1.45	0.0
20	4.57	1.47	0.65
21	1.44	1.50	0.65

[a] mol/s.

[b] cm measured with respect to the bottom of tube 2. Positive values indicate positions inside tube 2.

the sample passes out of view of the mirrors. The final sum gives the vibrational populations and the total emission intensities used in the comparison with the corresponding experimental data. At the bottom of the optical cell, the total pressure, final flow velocity, elapsed time, and mass balance are printed.

The calculation is initialized using a fourth order Runge–Kutta procedure, then carried out by a sixth order Adams–Moulton predictor corrector. The stiffness ratio of the rate equations is less than 10^6, hence this procedure provides adequate stability. The time step used in most calculations is 2.0×10^{-7} s. In all cases, the results are invariant to halving the time step.

The optimization of the parameters is carried out iteratively. First, the value of one parameter is varied slightly, the complete dataset simulated, and the rms deviation between the measured and observed values is calculated. This procedure is repeated twice more, and a parabola is computed through the three pairs of values of the rms deviation vs the parameter. The minimum in this parabola is used as the new estimate of the parameter, and the entire procedure is repeated for another parameter. This technique provides a sensitivity analysis for each parameter as it is optimized. The sensitivity information is available from the curvature of the parabola. The calculation is carried out on an LSI 11/23-based system equipped with hardware arithmetic. A single calculation of the 11 $F + H_2$ experiments mentioned above requires about 100 min. Optimization of the entire set of five parameters requires about 3–5 days.

In the construction of this model, it was intended that two of the five parameters (N_d and P_p) should be sensitive to the experimental apparatus, but independent of the molecular reagent being used. P_p should depend on the physical configuration of the injector and tube 2, while N_d, which describes the F atom production, should depend on such parameters as F atom precursor molecule and microwave power level. Simulation of several experiments similar to the one discussed in the next section has verified that N_d is constant with time (during an experiment) and changes insignificantly if tube 2 is replaced between experiments. (After replacement of tube 2, a CF_4 or SF_6 discharge is run for several hours in the new tube before it is used in the collection of data[18].)

The remaining parameters K_w^{-1}, K_w^0, and α_w, which describe wall deactivation, depend strongly upon the surface condition of the inlet glassware. For "clean" experiments, such as the $F + H_2$ discussed in the next section, these parameters are found to vary insignificantly with time and with replacement of inlet glassware. However, for reaction (1), a

TABLE II.[a] Measured vibrational distributions for experiments listed in Table I. Distributions in parentheses were computed using numerical model.

Run	$P(v'=0)$	$P(v'=1)$	$P(v'=2)$	$P(v'=3)$	P_{TOT}
11	···	0.32	0.49	0.19	0.08
	(0.04)	(0.32)	(0.48)	(0.20)	(0.03)
12	···	0.37	0.47	0.16	0.25
	(0.04)	(0.36)	(0.46)	(0.18)	(0.12)
13	···	0.40	0.45	0.15	0.33
	(0.04)	(0.40)	(0.43)	(0.17)	(0.23)
14	···	0.42	0.43	0.15	1.0
	(0.05)	(0.40)	(0.44)	(0.16)	(1.0)
15	···	0.39	0.45	0.16	0.67
	(0.04)	(0.37)	(0.45)	(0.18)	(0.53)
16	···	0.31	0.50	0.19	0.23
	(0.04)	(0.32)	(0.48)	(0.20)	(0.16)
17	···	0.30	0.51	0.19	0.06
	(0.04)	(0.31)	(0.49)	(0.20)	(0.05)
18	···	0.27	0.52	0.21	0.22
	(0.03)	(0.28)	(0.51)	(0.21)	(0.12)
19	···	0.34	0.48	0.18	0.46
	(0.04)	(0.34)	(0.48)	(0.18)	(0.48)
20	···	0.38	0.46	0.16	0.94
	(0.04)	(0.39)	(0.45)	(0.16)	(0.95)
21	···	0.40	0.45	0.15	0.30
	(0.04)	(0.39)	(0.44)	(0.17)	(0.23)

[a] Calculated populations are normalized such that $P(v'=1\text{–}3) = 1.0$ for ease of comparison with measured populations.

layer of solid NH_4F slowly forms on the inner surface of tube 2 as the experiment progresses, with the result that the wall deactivation pattern changes with time during the experiment. This change has very marked effects on the observed energy distribution pattern. In a later section, it will be shown that this effect is described very well by the parameter K_w^0.

B. Calibration of parameters

Eleven $F + H_2$ energy distribution measurements were carried out in order to obtain the measured data with which the calculated results could be compared. The results of the computations on these experiments are given in Tables II–IV. The experimental conditions under which the data were taken are recorded in Table I.

Table II shows the measured vibrational distributions from each experiment listed in Table I. Beneath each measured result is a calculated value in parentheses obtained in the optimization procedure previously described. The values of the parameters to which the optimization converged during this calibration are

$$N_d = 2.69, \quad P_p = 12.6\ \text{cm}, \quad K_w^0 = 0\ \text{s}^{-1},$$
$$K_w^{-1} = 8.8 \times 10^3\ \text{s}^{-1}, \quad \alpha_w = 3.0.$$

These five values produced all of the calculated results shown in Table II, and reproduced all subsequent measurements on $F + H_2$ in which the same reagent inlet device was used.

Table II shows that the simulation reproduced each vibrational population in the data set to within 2%, and the total populations to within about 15% of the reference run, No. 14. These limits are within the experimental error for the respective results. The total population (P_{TOT}) for a specific experiment is obtained by summing the measured populations for each HF state which was observed. Thus they do not include $P(v' = 0)$. The $P(v' = 0)$ were also omitted from the calculated P_{TOT} to be consistent. Because the absolute emission intensity is measured for each experiment, the relative values of the populations are obtained for the different experiments (runs). These are normalized to 1.0. The calculated populations are independently normalized to 1.0 as well.

The experimental errors which are most important are those in the measurement of reagent flows. The calculation shows that the total populations are very sensitive to the precise values used for these flows, but the energy distributions are less so. This is due to the fact that a change in a reagent flow causes two separate changes in the energy distribution which tend to cancel: Increasing a reagent flow increases the rate at which vibrationally excited product is created in the reaction, but it also increases the rate of product vibrational deactivation by the same reagent. In contrast, the total populations vary directly as the reagent flows without any cancellation. The reagent flow measurements have an uncertainty of ± 10%. Thus, the agreement shown in Table II is within this limit. We therefore conclude that the model provides a good representation of the behavior of the real system.

TABLE III. Inelastic rate constants used in the numerical model.

Relaxer	Rate ($v = 1 \to 0$) ($\text{Torr}^{-1}\,\text{s}^{-1}$)	Vibrational level scaling[a] $v = 2$	$v = 3$	$v = 4$
SF_6	1.0×10^3	2.0	7.0	12.6
H_2	1.5×10^4	0.86	0.79	1.20
HF	5.1×10^4	14.0	21.0	49.0
F	9.8×10^3	4.0	9.0	16.0
H	8.0×10^3	3.6	450.0	450.0

[a] Relative to rate for $v = 1 \to 0$.

Table III presents the values of the inelastic rate constants used in the calculation.[12,13] Only $\Delta v = -1$ processes were included in all cases. The rate constant used for the $F + H_2$ reaction was $7.94 \times 10^5\ \text{Torr}^{-1}\,\text{s}^{-1}$ (14). The primary energy distribution assumed is $P(v' = 0{:}1{:}2{:}3) = 0.02{:}0.17{:}0.55{:}0.26$.[15]

Two representative detailed simulation results are shown in Figs. 2 and 3 in the form of plots of the evolution of the vibrational distributions as a function of distance from the injector tip. Positive values indicate distances below the tip. Figure 2 shows run No. 13 (see Table I). Here the injector tip is located 0.65 cm inside tube 2. In Fig. 3 (run No. 17), it is 1.75 cm below the end of tube 2. The flows for the two experiments are the same and thus the differences in the distributions result from the different extents of wall and gas phase deactivation resulting from the change in location of the reaction zone. These plots make it clear that the reaction zone must be located far enough from the reagent inlet so that no deactivation can occur on its walls.

In normal operation of the low-pressure experiment with a clean reaction like $F + H_2$, the effects of deactivation by the walls of the reagent inlet device are not important since the reaction zone can be moved far enough from it simply by extending the injector. However, part of the unusual behavior observed for the $F + NH_3$ reaction can be shown to result from extremely efficient deactivation (to $v = 0$) in collisions of the HF(v) with the walls of the reagent

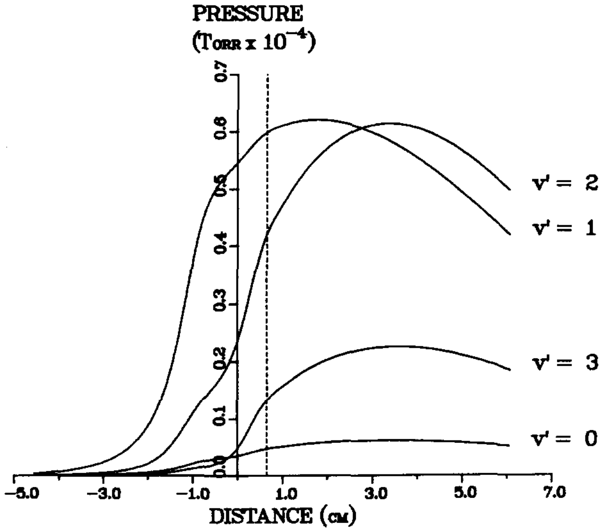

FIG. 2. Evolution of the partial pressures of the HF vibrational levels with distance down tube 2 for run No. 13 (Table II). The end of tube 2 is indicated by the dashed line. The injector tip is located at the origin of the horizontal axis, 0.65 cm inside tube 2.

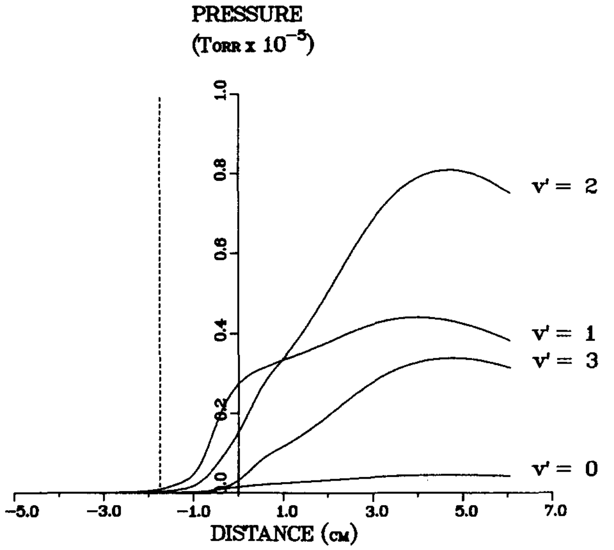

FIG. 3. See caption for Fig. 2. Evolution of HF partial pressures for run No. 17 the injector tip protrudes 1.75 cm below the end of tube 2.

inlets. In order to describe this effect, and to demonstrate that the calculation is capable of dealing with it, this wall deactivation process was included in the model via the parameter K_w^0. In the following section, the results of a calculation of this effect are compared with an experiment done to test it for the F/NH_3 system.

C. Calculation of wall deactivation effects

In our previous report of the energy distributions for the $F + NH_3$ and $F + ND_3$ primary reactions, we noted an unusual effect which occurred when the wall of the glass inlet tube became covered with NH_4F. This unusual behavior always occurs during experiments when the injector is located near or inside the end of tube 2. In this configuration the observed vibrational energy distribution is slightly relaxed due to collisions of the product with the walls of tube 2. However, if the same measurement is repeated several times (under identical experimental conditions) the observed vibrational energy distribution becomes less relaxed with each run.

We ascribe this effect to a change in the mechanism by which the vibrationally excited HF is deactivated in collisions with the walls, as the latter become coated with NH_4F. For collisions with a freshly prepared Teflon-coated quartz tube, vibrational relaxation of HF(v) is dominated by processes in which relatively small changes in the vibrational quantum number occur. This result was demonstrated in the modeling of the $F + H_2$ reaction reported in Table II, for which the best fit was obtained for $K_w^{-1} = 8.8 \times 10^3\ s^{-1}$ and $K_w^0 = 0.0\ s^{-1}$. However, in collisions with an NH_4F (or NH_3) coated surface, multiquantum relaxations (terminating in the $v' = 0$ level) predominate.

The experiment demonstrating this relaxation effect was reported in detail in Ref. 5. In that experiment, a single "standard" $F + H_2$ energy distribution measurement was repeated several times. Between runs, the amount of NH_4F deposited on the nearby wall of tube 2 was increased by running the $F + NH_3$ reaction in this tube for a short time. Since these observations are pertinent to the present paper they are reproduced in Table IV. For all of the experiments recorded in Table IV, the conditions were the same: SF_6 flow: 3.3 μmol/s, H_2 flow: 3.0 μmol/s, and injector location: 0.7 cm inside tube 2. Run No. 14 represents a base datum, taken under "clean wall" conditions before any NH_4F had been deposited. The subsequent $F + H_2$ distributions listed in Table IV differ only in the fact that slightly more NH_4F was deposited on the nearby wall of tube 2 between each replication of the measurement.

The populations in parentheses beneath the measured distributions were calculated using the numerical model. For run No. 14, the values of all five parameters obtained in the calibration procedure in the previous section were used without change. For runs 21–44, the value of K_w^0 was permitted to increase in order to describe the increasing importance of the ($v' \to 0$) process as the layer of NH_4 became larger. No other parameters were changed. The value of K_w^0 which gave each calculated result is listed in Table IV.

Table IV shows that for each measurement, the $F + H_2$ energy distribution becomes progressively more inverted, and the total intensity decreases. As reported in Ref. 5, it was verified that this effect was not due to any surface reaction involving NH_3 or NH_4F on the walls, by running control measurements of the $F + D_2$ reaction at regular intervals. No HF emission was observed in these control measurements.

The interpretation is as follows: before deposition of any NH_4F, the observed distribution (run 14) is substantially

TABLE IV. The effect on the observed distributions of NH_4F deposition on the inlet surfaces. The distributions in parentheses were computed using the numerical model.

Run	K_w^0	$P(v'=1)$	$P(v'=2)$	$P(v'=3)$	P_{TOT}
14	0.0	0.39	0.47	0.14	1.0
		(0.37)	(0.47)	(0.16)	(1.0)
21		0.35	0.48	0.17	0.70
	5.8×10^3	(0.35)	(0.48)	(0.17)	(0.92)
30		0.32	0.50	0.18	0.60
	1.4×10^4	(0.32)	(0.50)	(0.18)	(0.85)
35		0.30	0.52	0.18	0.45
	2.0×10^4	(0.30)	(0.51)	(0.19)	(0.81)
39		0.22	0.55	0.23	0.30
	8.9×10^4	(0.22)	(0.56)	(0.22)	(0.64)

TABLE V. Reference $F + H_2$ distributions measured during the experiments in which the F/NH_2 distributions were obtained. The distributions in parentheses were computed using the numerical model.

Run	SF_6 flow	$P(v' = 1)$	$P(v' = 2)$	$P(v' = 3)$	P_{TOT}
43	0.43	0.15	0.57	0.28	0.05
		(0.16)	(0.56)	(0.28)	(0.09)
39	2.9	0.16	0.56	0.28	0.22
		(0.17)	(0.56)	(0.27)	(0.28)
41	6.5	0.17	0.56	0.27	0.52
		(0.17)	(0.56)	(0.27)	(0.56)
45	17.4	0.18	0.56	0.26	1.0
		(0.19)	(0.56)	(0.25)	(1.0)

relaxed by collisions with the walls of tube 2. [The completely unrelaxed $F + H_2$ distribution is $P(v' = 1:2:3) = 0.17:0.56:0.27$.] As the deposition of NH_4F proceeds, processes of the type ($v \to v = 0$) become more probable, with the result that HF(v) molecules which strike the walls are converted to HF($v = 0$) and hence "disappear" from detection by the chemiluminescence (emission) experiment. There is thus a greater contribution to the observed distribution from those molecules which enter the light-collection optics without striking the wall; the intensity diminution is caused by the disappearance of those which do not.

Following the identification of this effect, several experiments were carried out to determine the conditions under which it could be eliminated. It was found that by extending the injector tip at least 2 cm below the end of tube 2, reproducable measurements could be obtained. Using this configuration, the $F + NH_2$ energy distribution described in the next section, was obtained.

IV. EXPERIMENTAL RESULTS AND DISCUSSION

The previous section dealt with results which were obtained for the $F + H_2$ reaction using the movable-injector reagent inlet apparatus. It was demonstrated that these results can be reproduced by a straightforward integration of the rate equations for the inelastic and reactive processes which are known to be occurring in the system. Also, it was shown that the same calculation reproduces accurately the unusually fast wall deactivation behavior which results when the reagent inlet becomes coated with NH_4F.

In this section, we report energy distributions for the F/NH_3 system measured under a wide variety of experimental conditions. Some of these conditions were designed to force the secondary reaction (2) to occur. Using the data from the latter experiments, and the numerical model (as calibrated in the previous section, but including rate equations for the secondary process as well) we calculate the separate contributions to the observed distributions, and hence extract the (unknown) vibrational distribution for the secondary reaction.

For the experimental conditions under which the secondary reaction is forced to occur in the apparatus used for this work, it is not possible to avoid the deposition of some NH_4F on walls of the reagent inlet. Since it is important that the observed distribution not change while a measurement is being made, the reagent inlet was saturated with NH_4F before the experiment was begun. As a result, futher deposition of NH_4F during the experiment could not change the wall deactivation pattern. It has been demonstrated in the last section that the ($v \to 0$) wall deactivation which results from this process can be adequately described by the use of the parameter K_w^0, without loss of accuracy in the numerical model calculations.

In addition to the evidence based on the behavior of K_w^0, an internal test was built into the experiment to verify directly that no change occurred in the wall deactivation pattern (or any other experimental parameter) during this series of measurements. This test was based on running the $F + NH_2$ measurements, as follows: For each experiment in this series, the NH_3 and H_2 are alternately switched into the injector, while a constant flow of F atoms is admitted *via* tube 1. (A small, constant flow of D_2 was also admitted *via* tube 2 in order to provide a further internal check, but this proved unnecessary as the behavior of the $F + D_2$ distributions was identical to that of the $F + H_2$ distributions in all cases.)

Each measurement was carried out by switching NH_3 into the injector, collecting 25 scans with the interferometer, then switching in H_2, collecting 25 scans, then back to NH_3 etc., until a total of 100 scans had been collected with each reagent. This procedure was then repeated for four different flows of F atoms. The distributions measured during the H_2 half of the cycle are shown in Table V. It is clear from these data that no change in the $F + H_2$ distributions occurred during the entire duration of the experiment. This observation demonstrates that no change in the wall deactivation pattern or the gas phase relaxation (by F atoms) resulted from the use of NH_3 or from the increase in the F atom flow.

As before, distributions calculated using the numerical model are shown in parentheses beneath the measured distri-

TABLE VI. Observed $F/NH_3/NH_2$ distributions used to determine the F/NH_2 distribution. The distributions in parentheses were computed using the numerical model.

Run	$P(v' = 1)$	$P(v' = 2)$	$P(v' = 3)$	$P(v' = 4)$	P_{TOT}
42	0.52	0.48	0.01	...	0.05
	(0.52)	(0.46)	(0.02)	...	(0.05)
38	0.51	0.47	0.02	...	0.22
	(0.47)	(0.49)	(0.03)	...	(0.22)
40	0.45	0.51	0.03	0.01	0.41
	(0.43)	(0.52)	(0.04)	(0.01)	(0.50)
44	0.39	0.54	0.05	0.02	1.0
	(0.42)	(0.53)	(0.04)	(0.01)	(1.0)

butions. For this calculation, the program was allowed to adjust (optimize) the values of the three parameters which described the wall deactivation processes: K_w^{-1} and α_w (the rate and v level power dependence of the $v \rightarrow v-1$ processes, respectively), and K_w^0 (the rate of the $v \rightarrow 0$ process). The values of the other parameters were not changed from those obtained in the calibration discussed in Sec. III B. Convergence was rapid to: $K_w^{-1} = 8.8 \times 10^3\ \text{s}^{-1}$ (the dependence on this parameter was very weak in the range $5–10 \times 10^3$), $\alpha_w = 0$, $K_w^0 = 5.0 \times 10^5\ \text{s}^{-1}$. Sections III A and III C show that these values are just the ones expected if the reagent inlet walls are heavily coated with an efficient relaxer. Table V shows that the observed $F + H_2$ distributions were reproduced accurately by these parameters. Thus, by using this procedure, the parameters describing the wall-related processes were obtained for the actual condition of the walls during this particular experiment.

The distributions for the secondary reaction were derived from the F/NH_3 data recorded alternately with the distributions shown in Table V. In order to calculate a distribution for the secondary reaction from data to which both reactions contribute, the distribution for the primary reaction must first be known. The latter, which was reported in Ref. 5, is $P(v' = 1{:}2) = 0.60{:}0.40$. Detailed experimental evidence is presented there to show that under the conditions of that measurement, *only* the primary reaction contributed to the observed distribution. Additional results to be presented later in this section, confirm that this primary distribution (when used in the numerical model with the secondary distribution to be derived momentarily) can accurately reproduce the entire range of distributions observed for this system, from the monotonically decreasing one just given, to the inverted ones, peaking in $v' = 2$, which can be easily observed for configurations in which the injector is withdrawn and the SF_6 flow is relatively high. Therefore, in what follows, the distribution from Ref. 5 will be taken as the primary one.

The $F + NH_3$ data which were taken alternately with the $F + H_2$ results, are shown in Table VI. The NH_3 flow was 2.7 μmol/s for all runs. The SF_6 flows were the same as for the respective runs in Table V. As indicated above, the calculated distributions shown in parentheses beneath the measured data in Table VI were obtained using the values of the parameters which were derived in the calculation of the $F + H_2$ data reported in Table V. However, for the calculated results shown in Table VI, rate equations describing both the primary and the secondary reactions [reactions (1) and (2) were included]. The total rates were taken to be: 2.0×10^{13} and $2.3 \times 10^{13}\ \text{cm}^3/\text{mol s}$ for the primary and the secondary reactions, respectively.[18] The (microscopic) rate constants used for the primary reaction were taken from Ref. 5. The calculation iterated on the set of (microscopic) rate constants for the secondary reaction, using the optimization technique described previously, until the calculated distributions matched the observed ones. The resulting values of the microscopic rate constants for the secondary reaction, together with the values used for the primary reaction, are listed in Table VII.

The data shown in Table VI demonstrate that these rate constants reproduce both the observed distributions and the total populations for the $F/NH_3/NH_2$ system quite accurately. The extra uncertainties which stem from the presence of two reactions in the system reduce the agreement between the observed and calculated distributions to $\pm 2\%$, which is not as high as that normally achieved in a single-reaction system ($\pm 1\%$).

TABLE VII.[a] Relative primary microscopic rate constants for the F/NH_3 and F/NH_2 reactions derived from the data in Table VI using the numerical model, calibrated with the data in Tables IV and V.

Reaction	$k(v' = 1)$	$k(v' = 2)$	$k(v' = 3)$	$k(v' = 4)$
(1)	0.60	0.40	···	···
(2)	0.23	0.68	0.08	0.01

[a] Estimated uncertainties are less than 0.05 in each vibrational level.

The validity of the microscopic rate constants shown in Table VII was also tested by using them to predict (accurately) the result of an experiment carried out to measure the primary distribution directly. For this experiment, freshly (Teflon) coated glassware was used, the injector was lowered until it protruded 3 cm below the end of tube 2 (to prevent interference from NH_4F deposition, as described in the previous section) and an SF_6 discharge was run in tube 2 for 2 h, following the standard procedure. Then, the power to the microwave discharge was reduced to the minimum which would sustain the plasma (to minimize the F atom concentration) and a single $F + NH_3$ experiment was carried out. The population distribution measured in this experiment was

$$P(v' = 1{:}2{:}3) = 0.62{:}0.37{:}0.01.$$

The numerical model was then used to calculate the result of this experiment, using the microscopic rate constants shown in Table VII. The parameters used for this calculation were

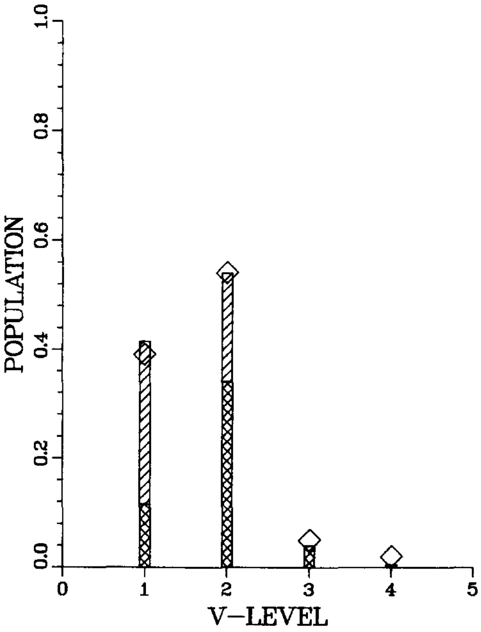

FIG. 4. Distribution for hypothetical case where each NH_2 radical produced in reaction (1) undergoes a secondary reaction. Single hatched region is contribution from reaction (1); crosshatching shows contribution from reaction (2). Points are the experimental results from run 44, Table VI.

those derived from the $F + H_2$ calibration described earlier and are appropriate to an experiment run under the lowest-attainable pressures, using clean glassware. In order to take account of the reduced power to the F atom discharge, the parameter N_d was reduced from 2.69 to 1.0. (It was found that for values of N_d below about 1.5, agreement within $\pm 1\%$ could be obtained, due to the very small contribution of the secondary reaction under these conditions.) The resulting calculated population distribution is

$$P(v' = 1{:}2{:}3) = 0.62{:}0.37{:}0.01.$$

This distribution, predicted using the relative microscopic rate constants of Table VII, with parameters from the appropriate calibration, correctly reproduces the measured distribution.

Finally, we can synthesize the hypothetical distribution which would result from the extreme case in which the F atoms are in such excess that each NH_2 radical reacts with an F atom before escaping from the reaction zone. The resulting distribution, which consists of equal contributions from both reactions, is $P(v' = 1{:}2{:}3{:}4) = 0.42{:}0.54{:}0.04{:}0.01$. This distribution is shown in Fig. 4. The single hatching indicates the contribution from the primary reaction; the doubly hatched portions are the contributions of the secondary reaction to each vibrational population. This distribution is very close to that observed in run 44, Table VI, for which the F atom flow (as calculated by the numerical model) was 17 times greater than the NH_3 flow. The latter experimental results are shown as points on the figure for comparison.

Although the synthetic distribution represented by the bars takes no account of gas phase or wall deactivation processes, it coincides closely with the experimentally measured points. This suggests that under the conditions of experiment 44, virtually every NH_2 reacts with an F atom. Furthermore, the heavily coated walls of the reagent inlets ensure that those vibrationally excited HF molecules which strike the walls, are efficiently deactivated to the ground vibrational state.

V. QUANTUM CHEMICAL RESULTS AND DISCUSSION

A. Computational methods

Preliminary calculations were performed with a modified version[19] of GAUSSIAN 80.[20] All results reported here were obtained with GAUSSIAN 82, Release A.[21] Geometries were optimized using gradient methods with the 4-31G split-valence basis set.[22] Analytical harmonic vibrational frequencies were calculated[23] to verify the natures of all stationary point structures and to compute zero-point vibrational energies. The reactants $F + NH_2$ and products $HF + NH$ were calculated within the supermolecule approach with the fragments separated by a large distance. The triplet state calculations were carried out within the unrestricted Hartree–Fock UHF framework.[24] Further computations were done at the 4-31G SCF geometries. The triply split valence plus polarization (on H, N, and F) 6-311G** basis set[25] was used in SCF and single plus doubles configuration interaction (CISD) calculations to yield more reliable energy differences. Two frozen core orbitals were excluded but all virtual orbitals included in the CISD computations. An estimate of the effect of higher excitations upon the CISD energy results was made by a size consistency correction (SCC).[26]

B. Results

The calculated total energies in hartree and relative energies in kcal mol^{-1} with respect to the reactants $F + NH_2$ at the various levels of theory are collected in Table VIII. The best estimated energy differences from the 6-311G** CISD + SCC results combined with corrections for zero-point vibration using the 4-31G harmonic frequencies are also illustrated in Fig. 5. The 4-31G UHF optimized geometry for the hydrogen abstraction reaction on the lowest triplet state and the normal mode of imaginary frequency corresponding to motion along the reaction coordinate are presented in Fig. 6.

The calculated energy difference between reactants and products at the 6-311G** CISD + SCC level and with con-

TABLE VIII. Total energies (E) in hartree and relative energies (ΔE) in kcal mol^{-1} with respect to the reactants $F + NH_2$ at various levels of computation. All calculations are at the 4-31G SCF optimized geometries.

		$F + NH_2$	NH_2F	$HNHF^{\ddagger}$	$HF + NH$
4-31G SCF	E	− 154.740 200	− 154.757 001	− 154.716 690	− 154.772 236
	ΔE	0.0	− 10.5	+ 14.8	− 20.1
ZPE corrected	E	− 154.716 312	− 154.724 546	− 154.696 948	− 154.750 527
	ΔE	0.0	− 5.2	+ 12.2	− 21.5
4-31G CISD	E	− 154.917 227	− 154.989 409	− 154.918 512	− 154.961 689
	ΔE	0.0	− 45.3	− 0.8	− 27.9
4-31G CISD + SCC	E	− 154.925 823	− 155.004 920	− 154.933 159	− 154.971 045
	ΔE	0.0	− 49.6	− 4.6	28.4
6-311G** SCF	E	− 154.975 285	− 155.004 260	− 154.950 433	− 155.022 050
	ΔE	0.0	− 18.2	+ 15.6	− 29.3
6-311G**CISD	E	− 155.293 152	− 155.380 425	− 155.295 486	− 155.354 703
	ΔE	0.0	− 54.8	− 1.5	− 38.6
6-311G**CISD + SCC	E	− 155.314 342	− 155.411 224	− 155.324 616	− 155.377 314
	ΔE	0.0	− 60.8	− 6.4	− 39.5

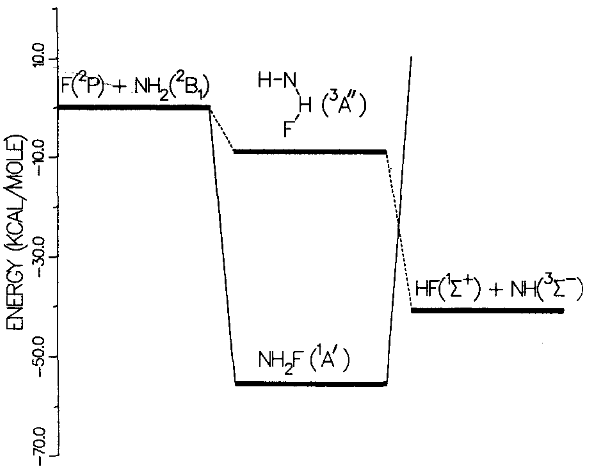

FIG. 5. Calculated energy differences based on the 6-311G** CISD + size consistency correction results. The values noted include the zero-point energies.

sideration of changes in zero-point vibrational energies is -40.9 kcal mol^{-1}. This calculated value is about 95% of the reaction exothermicity derivable from recommended experimental thermochemical data (-43 ± 5 kcal mol^{-1} [27]) and is well within the uncertainty in the latter value. NH_2F ($^1A'$) is predicted to be a deep well on the singlet surface with a stability of 55.5 kcal mol^{-1} (6-311G** CISD + SCC + Δ ZPE) relative to F + NH_2 and thus stable by 14.6 kcal mol^{-1} relative to the HF + NH products. There does not appear to be any direct thermochemical data on NH_2F ($^1A'$). An empirical bond energy analysis predicts NH_2F to be 64.5 kcal mol^{-1} more stable than F + NH_2 and 23.3 kcal mol^{-1} more stable than HF + NH.[28] Both these values are certainly compatible with the *ab initio* calculated results.

The most critical energy difference is that to the transition state for the direct hydrogen abstraction by F on the lowest triplet ($^3A''$) surface. If the inverted product vibrational distribution results from a direct abstraction mechanism on this triplet surface, the transition state must be energetically accessible to (room temperature) thermal reagents. At the 4-31G SCF level at which the geometries of the reactants and transition state were optimized this barrier is 14.8 kcal mol^{-1} and decreases slightly to 12.2 kcal mol^{-1} when zero-point vibrational energies are considered. The 6-311G** SCF barrier at the 4-31G geometry is of a similar magnitude, namely 15.6 kcal mol^{-1}. However, the CISD and SCC act to decrease the barrier height dramatically and in fact at the 4-31G SCF geometries used, the FHNH transition state falls to about 5 to 7 kcal mol^{-1} below reactants. The dramatic decrease when election correlation effects are included is clearly due to difficulties with a simple one-configuration SCF description of the unusual bonding in the transition structure. It is difficult to quantitatively assess the effects that reoptimization of the reactant and transition state structures at the CI level would have on this barrier height. However, it is clear that the barrier to the F + NH_2 reaction on the triplet surface is very small—almost certainly less than 5 kcal mol^{-1}, and possibly zero.

The geometry of the transition state structure (Fig. 6) and the harmonic vibrational frequencies at this point are of interest as a first connection between structure and dynamics. The harmonic vibrational frequencies at the 4-31G SCF level are collected in Table IX for all stationary points considered. The F + NH_2 and HF + NH frequencies refer to the supermolecules. The value of the frequencies scaled by 0.89 to allow both for anharmonicity and for the SCF approximation are also reported.[29]

The FH bond being formed and the undisturbed NH bond are *s-cis* in the transition structure. The F atom avoids the in-plane lone pair on N by such an approach. The transition structure for the abstraction of H from H_2 by NH($^3\Sigma^-$) has a similar conformation.[30] The one NH bond at 1.018 Å is roughly one-third of the way to its calculated value in the NH product (1.030 Å). The calculated NH distance in the NH_2 reactant was 1.014 Å. The HNH angle at the transition state (108.3°) is very close to its reactant value of 108.24°. The NH bond which is attacked by the F atom has stretched by $\sim 10\%$, to a value of 1.21 Å. The FH distance for the bond being formed in the reaction is 1.310 Å and thus is a full 0.388 Å or $\sim 40\%$ greater than the final calculated value in the HF product (0.922 Å). Thus the values of the bond lengths would suggest strong vibrational excitation of the HF product.

The values of the frequencies in Table IX confirm some of the above analysis of the transition state. The NH_a stretch at 3165 cm^{-1} (the scaled values will be used in this discussion) is very similar to the symmetric and asymmetric stretch values of 3137 and 3242 cm^{-1} in NH_2. The bending frequency for the HNH group in the transition state structure is 1452 cm^{-1}, which is only 25 cm^{-1} less than the corresponding mode in isolated NH_2. The a'' out-of-plane frequency 670 cm^{-1} confirms the planarity of the transition state structure. The vibrational mode with imaginary frequency which corresponds to motion along the reaction pathway at the transition state is $3346i$ cm^{-1} (or $2978i$ cm^{-1} if scaled). This mode is sketched in Fig. 6 and is clearly dominated by the motion of the hydrogen being abstracted.

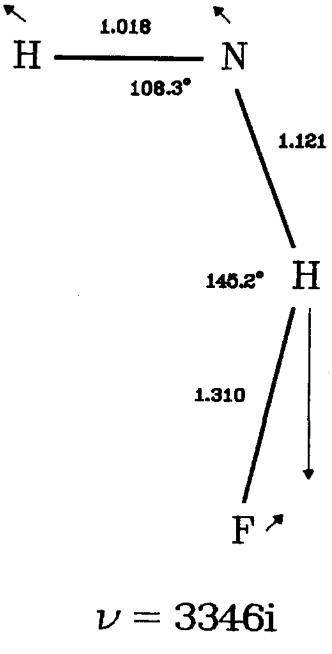

FIG. 6. The optimized geometry for the direct hydrogen abstraction on the $^3A''$ surface as determined at the 4-31G UHF level.

TABLE IX. 4-31G SCF harmonic vibrational frequencies. Sealed values result from multiplication of the calculated frequencies by 0.89 to allow for anharmonicity and the SCF approximation.

			4-31G SCF Harmonic frequency	Scaled	Experiment
$F + NH_2$	b_1 asym. str.		3643	3242	3280
	a_1 sym. str.		3525	3137	3280
	a_1 bend		1659	1477	2497
NH_2F	a'' NH_2 asym. str.		3821	3401	...
	a' NH_2 sym. str.		3686	3281	...
	a' NH_2 sym. deform		1793	1596	...
	a'' NH_2 asym. deform		1409	1254	...
	a'		1267	1128	...
	a'		998	888	...
$HF + NH$	a_1 HF str.		4118	3665	4138
	a_1 NH str.		3339	2972	3282
H_aNH_bF	transition	a' NH_a str.	3556	3165	...
	structure	a' H_aNH_b	1632	1452	...
		a'	913	813	...
		a'' out-of-plane	753	670	...
		a'	339	302	...
		a' FH_b str.	$3346i$	$2978i$	...

VI. CONCLUSION

We have presented evidence which demonstrates several properties of the energy partitioning in the F/NH_3 system. When the reaction is carried out under conditions where only the primary $F + NH_3$ step would be expected, the observed HF vibrational distribution is cold, and the maximum populated level is $v' = 2$, consistent with the thermochemical limit imposed by this reaction. When the conditions are altered to favor the occurrence of the secondary $F + NH_2$ reaction as well, the observed HF vibrational distribution becomes inverted, and the maximum populated HF vibrational level becomes $v' = 4$, which cannot be produced by the primary step, but is accessible to the secondary atom/radical reaction. Numerical simulation of the experiment quantitatively reproduces all observed results when the model includes both the primary and secondary reactions. No qualitative agreement can be achieved if the atom/radical reaction is not included in the model. The calculation shows that the vibrational distribution of the HF produced in the atom/radical reaction is strongly inverted, peaking in $v' = 2$.

Ab initio quantum chemical calculations show that the energy of the transition state corresponding to reaction on the lowest triplet surface is approximately the same as that of the reagents, and reaction on this surface is thus possible for the room temperature thermal reagents used in these experiments. This is in contrast to the isoelectronic $F + OH$ reaction, for which this triplet surface is energetically inaccessible. For the $F + NH_2$ reaction, the triplet surface describes a direct abstraction, proceeding through a bent FHNH intermediate, and correlating directly with the ground state reagents. We conclude that this is the major pathway for the $F + NH_2$ reaction, or at least that part of it which produces vibrationally excited HF. Since there is no potential energy well on this surface corresponding to a bound intermediate, the reaction has simple, direct dynamics, leading to strong vibrational inversion of the produce HF.

The conclusions reported here for the $F/NH_3/NH_2$ systems are all equally valid for the $F/ND_3/ND_2$ reactions as well. The observed experimental behavior of the latter system mimics that of the former in all respects, including the dependencies on reagent flows and wall deactivation reported in earlier sections of this paper. A detailed report of this identical behavior was given in Ref. 5. Only one aspect of the F/ND_3 results needs specific discussion here. The lowest-pressure (hence least perturbed by relaxation and secondary reaction) energy distributions reported in Ref. 5 for the NH_3 and ND_3 systems, respectively were $P(v' = 1{:}2) = 0.60{:}0.40$ and $P(v' = 1{:}2{:}3) = 0.36{:}0.27{:}0.37$. In the present report, we demontrated that the initial distribution for the F/NH_3 reaction must be either the same as or colder than the one reported in Ref. 5. (The initial distribution would be colder if we were unable to completely eliminate the secondary reaction in the experiments.) The experimental evidence presented in Ref. 5 indicates that at least for the F/NH_3 system, the secondary reaction was eliminated.

We have also reported in Ref. 5 that he "*V*"-shaped distribution obtained for the F/ND_3 reaction is *not* the initial one because the observed vibrational populations were still changing with changes (decreases) in the total pressure and reagent flows at the lowest-pressure conditions achievable for the F/ND_3 system. The pressure could not be decreased as much for the F/ND_3 system as for the F/NH_3 system because the Einstein transition probabilities of DF are a factor of 4 smaller than those of HF.

The *direction* of the changes in the F/ND_3 distribution, however, were the same as those for the F/NH_3 distribution: as the reaction zone pressure is decreased, the population of $DF(v' = 3)$ decreases rapidly, that of $DF(v' = 2)$ decreases more slowly, and that of $DF(v' = 1)$ decreases least. This trend is shown in Fig. 8 of Ref. 5, which gives the measured distributions as a function of the flow of F atoms. This shows that if the concentration of F atoms in the reaction zone could be decreased sufficiently, a monotonically decreasing F/ND_3 distribution like that observed for F/NH_3 would be obtained. We therefore conclude that the energy distributions produced by the F/NH_3 and F/ND_3 reactions are the same; they are both monotonically decreasing with increasing vibrational excitation.

We further conclude that as the concentration of F atoms in the reaction zone increases, the very rapid secondary reactions begin to occur in both cases. These produce inverted vibrational distributions in the diatomic products, giving overall observed vibrational distributions which are more inverted than those of the primary reaction alone.

[1] W. H. Duewer and D. W. Setser, J. Chem. Phys. **58**, 2310 (1973).

[2] D. J. Douglas and J. J. Sloan, Chem. Phys. **46**, 307 (1980).

[3] J. J. Sloan, D. G. Watson, and J. Williamson, Chem. Phys. Lett. **74**, 481 (1980).

[4] A. S. Manocha, D. W. Setser, and M. A. Wickramaaratchi, Chem. Phys. **76**, 129 (1983).

[5] D. J. Donaldson, J. Parsons, J. J. Sloan, and A. Stolow, Chem. Phys. **85**, 47 (1984).

[6] (a) J. J. Sloan, D. G. Watson, J. M. Williamson, and J. S. Wright, J. Chem. Phys. **75**, 1190 (1981); (b) D. J. Donaldson, J. S. Wright, and J. J. Sloan, Can. J. Chem. **61**, 912 (1983).

[7] (a) J. J. Sloan and D. G. Watson, J. Chem. Phys. **74**, 744 (1981); (b) D. J. Donaldson, D. G. Watson, and J. J. Sloan, Chem. Phys. **68**, 95 (1982); (c) D. J. Donaldson and J. J. Sloan, J. Chem. Phys. **77**, 4777 (1982).

[8] D. J. Donaldson and J. J. Sloan, Can. J. Chem. **61**, 906 (1983).

[9] E. Zamir and R. D. Levine, Chem. Phys. **52**, 253 (1980), and references therein.

[10] A. Roth, *Vacuum Technology* (North-Holland, Amsterdam, 1976).

[11] (a) J. A. Giordmaine and T. C. Wang, J. Appl. Phys. **31**, 463 (1959); (b) J. C. Johnson, A. T. Stair, Jr., and J. L. Pritchard, *ibid.* **37**, 1551 (1966).

[12] L. S. Dzelzkalns and F. Kaufman, J. Chem. Phys. **77**, 3508 (1982).

[13] S. R. Leone, J. Phys. Chem. Ref. Data **11**, 953 (1982).

[14] E. Wurzberg and P. L. Houston, J. Chem. Phys. **72**, 4811 (1980).

[15] B. E. Holmes and D. W. Setser, in *Physical Chemistry of Fast Reactions, Vol. 2. Reaction Dynamics*, edited by I. W. M. Smith (Plenum, New York, 1980).

[16] R. O. Waddoups, AFCRL Scientific Report No. 3, Air Force Cambridge Research Laboratories, Bedford, MA, 1966.

[17] M. A. A. Clyne and A. H. Curran, in *Gas Kinetics and Energy Transfer*, edited by P. G. Ashmore and R. J. Donovan (The Chemical Society, London, 1977), Vol. 2.

[18] C.-D. Walther and H. Gg. Wagner, Ber. Bunsenges. Phys. Chem. **87**, 403 (1983).

[19] M. R. Peterson and R. A. Poirier, MONSTERGAUSS, Department of Chemistry. University of Toronto, Toronto, Canada, 1981.

[20] J. S. Binkley, R. A. Whiteside, R. Krishnan, R. Seeger, D. J. DeFrees, H. B. Schlegel, S. Topiol, L. R. Kahn, and J. A. Pople, GAUSSIAN80, Department of Chemistry, Carnegie-Mellon University, Pittsburgh, 1981.

[21] J. S. Binkley, M. Frisch, K. Raghavachari, D. DeFrees, H. B. Schlegel, R. Whiteside, E. Fluder, R. Seeger, and J. A. Pople, GAUSSIAN82. Release A, Department of Chemistry, Carnegie-Mellon University, Pittsburgh, 1983.

[22] R. Ditchfield, W. J. Hehre, and J. A. Pople, J. Chem. Phys. **54**, 724 (1971).

[23] J. A. Pople, R. Krishnan, H. B. Schlegel, and J. S. Binkley, Int. J. Quantum Chem. Symp. **13**, 225 (1979).

[24] J. A. Pople and R. K. Nesbet, J. Chem. Phys. **22**, 571 (1954).

[25] R. Krishnan, J. S. Binkley, R. Seeger, and J. A. Pople, J. Chem. Phys. **72**, 650 (1980).

[26] J. A. Pople, R. Seeger, and R. Krishnan, Int. J. Quantum Chem. Symp. **11**, 149 (1977).

[27] (a) H. Okabe, *Photochemistry of Small Molecules* (Wiley, New York, 1978); (b) H. M. Rosenstock, K. Draxl, B. W. Steiner, and J. T. Herron, J. Phys. Chem. Ref. Data **6**, 774 (1977).

[28] L. Pauling, *The Nature of the Chemical Bond*, 3rd ed. (Cornell University, Ithaca, 1960).

[29] J. A. Pople, H. b. Schlegel, R. Krishnan, D. J. DeFrees, J. S. Binkley, M. J. Frisch, R. A. Whiteside, R. F. Hout, and W. J. Hehre, Int. J. Quantum Chem. Symp. **15**, 269 (1981).

[30] T. Fueno, V. Bonacic-Koutecky, and J. Koutecky, J. Am. Chem. Soc. **105**, 5547 (1983).